

A NOTE ON BIMODAL ACCRETION DISKS

C.P. DULLEMOND
Leiden Observatory,
P.O. Box 9513, 2300 RA Leiden, The Netherlands
e-mail: dullemon@strw.leidenuniv.nl
AND

R. TUROLLA
Dept. of Physics, University of Padova,
Via Marzolo 8, 35131 Padova, Italy
e-mail: turolla@astaxp.pd.infn.it
Draft version August 26, 2018

ABSTRACT

The existence of bimodal disks is investigated. Following a simple argument based on energetic considerations we show that stationary, bimodal accretion disk models in which a Shakura–Sunyaev disk (SSD) at large radii matches an advection dominated accretion flow (ADAF) at smaller radii are never possible using the standard slim disk approach, unless some extra energy flux is present. The same argument, however, predicts the possibility of a transition from an outer Shapiro–Lightman–Eardley (SLE) disk to an ADAF, and from a SLE disk to a SSD. Both types of solutions have been found. We show that for any given accretion rate a whole family of bimodal SLE–ADAF and SLE–SSD solutions can be constructed, each model being characterized by the location of the transition radius.

Subject headings: accretion, accretion disks — black hole physics — hydrodynamics

1. INTRODUCTION

Observations of black hole X–ray binaries (BHXBs, e.g. V404 Cyg, Nova Muscae, A0620-00, GRO J1655-40, Cyg X-1) suggest that a bimodal accretion disk may be present in these sources (Thorne & Price 1975; Shapiro, Lightman & Eardley 1976; Narayan, McClintock & Yi 1996; Esin, McClintock & Narayan 1997). The inner part is a hot, optically thin, quasi–spherical accretion flow, producing a non–thermal spectrum via synchrotron radiation and Comptonization, with a cut–off around 100 keV. The outer part is a geometrically thin, optically thick disk (Shakura & Sunyaev 1973; Frank, King & Raine 1992) which emits a multi–color blackbody spectrum peaked around a few keV. By making plausible assumptions on how the transition radius R_{tr} depends on the accretion rate \dot{M} , one obtains a one–parameter family of spectra, once the black hole mass M and the viscosity parameter α are specified. The different spectral states of the BHXBs can then be explained by varying the accretion rate $\dot{M} = \dot{m}\dot{M}_{Edd}$, where \dot{M}_{Edd} is the Eddington accretion rate.

Historically the hot, inner region was first thought to be a cooling–dominated, optically thin accretion disk, the SLE disk (Shapiro, Lightman & Eardley 1976, henceforth SLE). However, such disks are subject to a violent thermal instability, which makes them useless for constructing stationary bimodal models. An alternative to the SLE disk could be the recently discovered hot, advection dominated accretion flows (ADAFs: Narayan & Yi 1994, 1995; Abramowicz et al. 1995), which are stable against both thermal and viscous perturbations. ADAF models have been quite successful in reproducing the spectral properties of BHXBs in quiescence and of the Galactic center source Sgr A* (Narayan, Yi & Mahadevan 1995). A bimodal disk structure, in which an outer Shakura–Sunyaev

disk (SSD) connects smoothly to the inner ADAF, seems very promising in explaining the whole range of spectral states of BHXBs, from the quiescent to the high state (Esin, McClintock & Narayan 1997).

Advection dominated accretion flows are dynamically very stable. The robustness of the ADAF solutions led Narayan & Yi (1995) to suggest that perhaps nature will always select this option whenever it becomes available. Yet, the precise mechanism through which the SSD material is converted into an ADAF remains a matter of debate. Observations of Cyg X-1 in the low state suggested that the transition from a cold to a hot disk might result from the secular instability of the radiation–pressure dominated inner part of the SSD (SLE; Ichimaru 1977). The even more violent thermal instability of the radiation–pressure dominated region (Pringle, Rees & Pacholczyk 1973; Piran 1978) might also be held responsible for such a transition. The drawback is that the transition radius for these models is usually quite close to the black hole, $R_{tr} \simeq 45\alpha^{2/21}\dot{m}^{16/21}m_*^{2/21}R_g$, where $m_* \equiv M/M_\odot$ and $R_g = 2GM/c^2$ is the Schwarzschild radius (SLE; Frank, King & Raine 1992), whereas observations of many BHXBs (e.g. Narayan, Barret & McClintock 1997; Hameury et al. 1997) seem to imply a transition radius $R_{tr} \sim 10^4 R_g$. Moreover, no self–consistent global solution for such a viscously/thermally driven transition has been found so far, and, more probably, the thermal instability results in a genuinely time–dependent behavior (e.g. a limit cycle, see Meyer & Meyer–Hofmeister 1981, Mineshige & Wheeler 1989; Honma, Matsumoto & Kato 1993; Szuszkiewicz & Miller 1997a, b), rather than in a stationary transition to a hot flow. More promising in this respect are the evaporation models in which matter evaporates from the SSD forming an advection dominated corona (Meyer & Meyer–Hofmeister 1994; Narayan & Yi

1995).

The question remains whether we understand why it seems not to be possible to convert an SSD directly into an ADAF at a certain radius. This is the question we address in this paper. We use a simple argument based on energetics to predict which kind of bimodal disk structures should be possible. We conclude that only bimodal accretion flows which are formed by a SLE disk outside and by an ADAF or SSD inside are allowed. We confirm our qualitative prediction by actually constructing global models for both bimodal SLE–ADAF and SLE–SSD solutions.

2. THE EQUATIONS

The system of equations governing the disk structure used in the present investigation are basically those of slim disks (Abramowicz et al. 1988) and our approach follow closely those used by Narayan, Kato & Honma (1997) and Chen, Abramowicz & Lasota (1997) in investigating the properties of global ADAF solutions. More specifically, we assume that the disk is stationary, axisymmetric, that the gravitational field of the central object is described by the pseudo-Newtonian potential $\Phi = -GM/(R - R_g)$ (Paczynski & Wiita 1980) and that self-gravity is completely negligible. Contrary to Narayan, Kato & Honma, we include radiative cooling in our equations, using the approximate expressions for bremsstrahlung losses given by Narayan & Yi (1995), which are valid at any optical depth. Although we expect optically thin bremsstrahlung cooling and gas pressure support to be adequate for consistently modeling the SLE–ADAF, the Shakura–Sunyaev disk in SLE–SSD models may be optically thick and radiation pressure dominated, so we include radiation pressure in our calculations.

By denoting the total pressure and the mass density at the equatorial plane with p and ρ , the corresponding vertically-integrated quantities are given by

$$P = 2Hp, \quad \Sigma = 2H\rho \quad (1)$$

where H is the half-thickness of the disk. The pressure p is the sum of gas and radiation pressure

$$p = p_g + p_r, \quad (2)$$

$$p_g = \frac{\mathcal{R}}{\mu} \rho T \quad (3)$$

where T is the average temperature of electrons and ions

$$T = \mu \left(\frac{T_i}{\mu_i} + \frac{T_e}{\mu_e} \right) \quad (4)$$

and for simplicity we take $\mu_i = \mu_e = 1$, $\mu = 0.5$. We allow T_i and T_e to deviate, but instead of using a sophisticated model for electron–ion coupling we just assume $T_e = \min(T_i, 6 \times 10^9 \text{ K})$. Following Abramowicz et al. (1996), we adopt for the radiation pressure the expression

$$p_r = \frac{Q_-}{4c} \left(\tau + \frac{2}{\sqrt{3}} \right) \quad (5)$$

where Q_- is the cooling rate and τ is the total optical depth (see below). Although in principle also magnetic pressure should be accounted for, this effect, like all other

effects of the frozen-in B -field, will be ignored in this paper. The isothermal sound speed c_s is given by

$$c_s^2 = \frac{P}{\Sigma} = \frac{p}{\rho} \quad (6)$$

and, following the standard approach, the disk thickness and the kinematic viscosity are expressed as

$$H = \frac{c_s}{\Omega_K}, \quad (7)$$

$$\nu = \frac{2}{3} \alpha c_s H \quad (8)$$

where Ω_K is the Keplerian rotational frequency, calculated using the pseudo-Newtonian potential. Introducing the radial velocity v_R and the angular velocity Ω , the continuity, radial momentum, azimuthal momentum and energy equations take the form

$$\dot{M} = -2\pi \Sigma R v_R, \quad (9)$$

$$-v_R \frac{dv_R}{dR} + (\Omega^2 - \Omega_K^2) R - \frac{1}{\rho} \frac{dp}{dR} = 0, \quad (10)$$

$$\Sigma R v_R \frac{d(R^2 \Omega)}{dR} = \frac{d}{dR} \left(\Sigma \nu R^3 \frac{d\Omega}{dR} \right), \quad (11)$$

$$\Sigma v_R \left(\frac{de}{dR} + p \frac{d\rho^{-1}}{dR} \right) = Q_+ - Q_-. \quad (12)$$

We adopt for the specific internal energy (including radiation) an equation of state of the form $(\gamma - 1)e = p/\rho = c_s^2$ with constant adiabatic index. In the energy equation (eq.[12]), the viscous heating Q_+ has the usual expression

$$Q_+ = \nu \Sigma \left(R \frac{d\Omega}{dR} \right)^2, \quad (13)$$

while the cooling rate Q_- is calculated using a bridging formula valid both in the optically thin and optically thick regimes (Narayan & Yi 1995),

$$Q_- = 8\sigma T_e^4 \left(\frac{3\tau}{2} + \sqrt{3} + \frac{8\sigma T_e^4}{Q_-^{br}} \right)^{-1}. \quad (14)$$

Here τ is the total (scattering plus absorption) depth

$$\tau = \tau_{es} + \tau_{abs} \quad (15)$$

and

$$\tau_{es} = \frac{1}{2} \kappa_{es} \Sigma, \quad (16)$$

$$\tau_{abs} = \frac{Q_-^{br}}{8\sigma T_e^4}. \quad (17)$$

The bremsstrahlung cooling function is expressed as (Narayan & Yi 1995)

$$Q_-^{br} = 2Hq_-^{br} = 8.5 \times 10^{25} H \rho^2 f_{ei} \text{erg cm}^{-2} \text{s}^{-1} \quad (18)$$

where

$$f_{ei}(\theta_e) = 4 \left(\frac{2\theta_e}{\pi^3} \right)^{\frac{1}{2}} (1 + 1.781 \theta_e^{1.34}) \quad (19)$$

and $\theta_e = kT_e/m_e c^2$ is the dimensionless electron temperature.

3. BIMODAL DISKS: ENERGETICS

The structure of accretion disks is determined by the set of differential equations given in section 2. In the case of geometrically thin disks these equations become algebraic, so that the disk properties may be evaluated locally (see e.g. Frank, King & Raine 1992). Although this is not true any more for geometrically thick disks, a good estimate of their structure may be nevertheless obtained from local considerations (see e.g. Abramowicz et al. 1995).

In the analysis of the global behaviour of the models, a key role is played by the energy equation, which simply states that viscous heating, radiative cooling and radial energy advection must balance at any radius

$$Q \equiv Q_+ - Q_- - Q_{adv} = 0. \quad (20)$$

The non-locality of equation (20) is contained in both Q_{adv} and Q_+ , which are functions of the gradients. For a standard thin disk, however, $Q_{adv} \simeq 0$ and $Q_+ \propto \dot{m}$, while for the other classes of disks they can be reasonably well approximated in terms of local variables. With this proviso, the energy equation, at any given radius, may be written as a function of \dot{m} and Σ : $Q = Q(\Sigma, \dot{m})$. The energetically permitted configurations are then given by the intersection of the surface $Q(\Sigma, \dot{m})$ with the $Q = 0$ plane, as shown in figure 1 (see e.g. Abramowicz et al. 1995; Chen et al. 1995). The curve on the left corresponds to ADAFs (upper branch) and SLE disks (lower branch), the S-shaped curve to ‘slim disks’ (upper branch), radiation pressure supported SSD (middle branch) and gas pressure supported SSD (lower branch).

Two of the five branches of accretion disks are well known to be thermally unstable, as can be easily inferred from figure 1. The unstable branches are those for which $Q_+ > Q_-$ above and $Q_+ < Q_-$ below the curve. For a solution on the radiation pressure supported SSD or SLE branch, a sudden local heating (which amounts to a vertical upward displacement in the $\log \Sigma - \log \dot{m}$ diagram) causes the disk to enter a region where heating exceeds cooling ($Q_+ > Q_-$). This results in more heating and a runaway thermal instability sets in. A local cooling of the unstable disk similarly produces a runaway cooling. Although the plot of figure 1 refers to the low viscosity case, the same conclusions hold for large values of $\alpha \sim 0.2 - 1$, when the topology of the solutions in the $\log \Sigma - \log \dot{m}$ plane changes (a very clear example can be found e.g. in Abramowicz & Lasota 1995).

In the rest of this section we show how the $\log \Sigma - \log \dot{m}$ diagram can be used also to identify the possible classes of bimodal, stationary flows, i.e. two types of disks connected by a boundary layer. Although the following analysis is somewhat qualitative, it leads to rather interesting conclusions which are confirmed by the numerical calculations discussed in sections 4 and 5. Let us consider again the energy equation. Using the exact (differential) expression for Q_{adv} , but retaining a ‘local’ approximation for Q_+ , equation (20) becomes

$$Q_{adv} = \Sigma v_R T \frac{ds}{dR} = Q_+ - Q_- \quad (21)$$

where s is the specific entropy. In a stationary flow $v_R ds/dR$ is just the Lagrangian rate of change of the spe-

cific entropy of a gas element (in the case under examination, a ‘vertically-integrated’ thin ring). Suppose now that the gas parcel is located at a given radius and that it has a specified value of $s = s_0$. Assume, just for concreteness, that s_0 is such that the configuration lies a bit to the left of the stable SSD branch of figure 1, so that it is $Q_+ < Q_-$. As time elapses, viscous stresses cause the gas parcel to move inwards and, since \dot{m} is constant, this amounts to a horizontal shift in the $\log \Sigma - \log \dot{m}$ diagram. Because cooling exceeds heating, the specific entropy must decrease in time and this implies that the configuration moves to the right, i.e. towards the curve. If the element is initially to the right of the branch, heating exceeds cooling, s increases in time and the gas parcel shifts again towards the SSD branch. One can then conclude that, even if the flow is not in the SSD phase at a certain radius, it will try to become a SSD for smaller radii. The same reasoning holds both for the stable and for the unstable SSD branches, since, in both cases, one has $Q_+ < Q_-$ to the left and $Q_+ > Q_-$ to the right of the curve. A major consequence is that stationary, bimodal accretion flows which consists of an outer SSD and a different kind of flow at smaller radii seem not to be allowed.

When applied to the SLE branch, however, this argument yields just the opposite result. Now it is $Q_+ < Q_-$ to the right and $Q_+ > Q_-$ to the left of the curve, so, unless it lies exactly on the SLE branch, the spiraling-in matter moves away from the curve. Depending on the initial value of the entropy, it will end either on the ADAF or on the SSD branch. Bimodal, stationary SLE-ADAF and SLE-SSD models seem therefore possible, in the sense that they are at least energetically permitted.

The same conclusions may be drawn looking at the integral curves of equation (21), which are shown in figure 3. By integrating equation (21) inwards, starting close to the SLE branch, the solutions diverge exponentially, until either the ADAF or the SSD branch is reached. This is the stationary transition from a SLE to either an ADAF or a SSD. A similar transition cannot be found starting from a SSD/ADAF and integrating inwards, because now the solutions exponentially relax back onto the SSD/ADAF branch.

In general one can say that disks on a branch with $Q_+ > Q_-$ on its left and $Q_+ < Q_-$ on its right can perform a stationary transition to a different state towards smaller radii, while disks on a branch with $Q_- > Q_+$ on its left and $Q_- < Q_+$ on its right can not, as illustrated in figure 2. Much as in the case of the stability analysis (see above), the same considerations apply to high- α flows (as can be easily verified from figure 1 of Abramowicz & Lasota 1995), so our result is independent of the viscosity parameter. Clearly, the inclusion of some extra (non-local) heating/cooling process in the energy equation changes the picture outlined above. As shown by Honma (1996) and Meyer & Meyer-Hofmeister (1994), convection and electron conduction may indeed provide a way to obtain global SSD-ADAF models.

The analysis presented in this section relies on the tacit assumption that none of the branches change as we follow the evolution of a gas element towards smaller radii. Of course this is not entirely true, since, at variance with what is done in the classical stability analysis, the radial coordinate of the gas parcel now varies because matter is spi-

raling in. Strictly speaking, one should draw many curves on the $\log \Sigma - \log \dot{m}$ diagram, each referring to the different radii crossed by the gas element. We note, however, that the time over which the topology of the $\log \Sigma - \log \dot{m}$ diagram changes is the viscous time of radial motion. The gas element evolves on a thermal timescale which is much shorter than the viscous time scale, so the small deformation of the curves can be safely ignored to first order. Much more delicate is the assumption that Q_+ can be evaluated in terms of local variables. In the transition region the derivative of Ω may deviate strongly from its usual value, casting some doubts on our conclusions. A strong test for the simple argument presented above is to actually construct the bimodal solutions for the cases in which transitions *are* allowed, by solving the full set of differential equations. Both the global SLE–ADAF and SLE–SSD solutions have been found numerically and are presented in sections 4 and 5.

4. BIMODAL SLE–ADAF FLOWS

In this section we present our numerical models for bimodal SLE–ADAF disks. We construct solutions which are in the ADAF phase for small radii and in the SLE phase for large radii. We shall show that the radius R_{tr} at which the transition occurs is a free parameter, with the only limitation that it must be $R_{tr} < R_{max}$. The existence of a maximum transition radius follows from the fact that, for too large radii, radiative cooling becomes too strong to allow of a hot, optically thin solution. A rough estimate of R_{max} may be found by equating the viscous heating to the optically thin bremsstrahlung cooling (eqs. [13] and [18]) and giving reasonable guesses of the values of $v_R(R)$, $c_s(R)$ and $\Omega(R)$ for an ADAF (Abramowicz et al. 1995),

$$R_{max} \sim 2 \times 10^4 \frac{\alpha^4}{\dot{m}^2} R_g. \quad (22)$$

Sufficiently within this radius bimodal stationary solutions, which are SLE for $R_{tr} < R < R_{max}$ and ADAF for $R < R_{tr}$, exist.

Equations (10, 11, 12) form a fourth order set of differential equations. We write the second order angular momentum equation (11) as two first order equations and solve the resulting four coupled differential equations numerically using a Henyey–type relaxation scheme (Nobili & Turolla 1988). Since we do *not* use the first integral of equation (11), the specific angular momentum at the inner edge, ℓ_0 , does not appear explicitly as an eigenvalue (see e.g. Narayan, Kato & Honma 1997), but follows from the solution once suitable boundary conditions have been specified. Logarithmic variables are adopted throughout: $\ln r$, where $r = 2R/R_g$, $\ln(v_R/c)$, $\ln(c_s/c)$, $\ln(\Omega/\Omega_K)$ and $d \ln \Omega / d \ln r$.

Global ADAF models are transsonic (see e.g. Narayan, Kato & Honma 1997; Chen, Abramowicz & Lasota 1997) and we expect also the bimodal solutions we are looking for to pass through a critical point close enough to inner rim. The location of the sonic point is an eigenvalue of the problem and follows once all boundary conditions are specified. The Henyey solver we use is specifically designed to locate critical points automatically, looking for the points where the Jacobian of the system changes sign. When a critical point is met, the solver replaces one of the

boundary condition with a regularity condition. Like in all relaxation–type schemes, a trial solution must be supplied to start the iteration. Usually its exact form is not very important, the only strong requirement being that the initial guess is transsonic. In the present case, we first generated a global ADAF model, using a modified self–similar solution as first guess, and then used it as the trial solution for the bimodal disk.

Although different values of the disk parameters were tested, models discussed here were obtained for $\alpha = 0.1$, $\gamma = 1.5$, $\dot{m} = 10^{-3}$ and $m_* = 10$. The inner and outer edges of the disk are located at $R_{in} = 1.5R_g$ and $R_{end} = 10^6 R_g$, respectively. An equally spaced logarithmic radial grid was used with $N \sim 300$ points. Grid–refinement was used to obtain better spatial resolution in the transition region.

4.1. The Boundary Conditions

In order to clarify the choice of the boundary conditions, let us start discussing how boundary conditions should be placed for a global ADAF solution in our scheme. Since the structure equations translate into four first order ODEs, four conditions are needed. As discussed above, the Henyey solver automatically puts one of these conditions (a regularity condition) at the critical point, which is automatically located. If a fine enough grid is used, any constraint which forces the derivatives to stay finite at the sonic radius will do. The remaining three conditions can be placed at either R_{in} or R_{out} . As discussed e.g. by Narayan, Kato & Honma (1997) the inner boundary condition must require the specific angular momentum, ℓ , to behave physically. At R_{in} , we ask that $d\ell/dR = 0$, which is equivalent to $d \ln \Omega / d \ln R = -2$. The last two conditions are given at the outer edge, specifying the values of c_s and Ω at R_{out} (see again Chen, Abramowicz & Lasota 1997 and Narayan, Kato & Honma 1997).

For the bimodal solutions we investigate in this paper, the outer disk is of the SLE type. Such a disk allows only one boundary condition at the outer edge, and the remaining condition must be specified elsewhere. This is a somewhat subtle point which will be discussed below.

4.2. The Solutions

In order to compute the SLE–ADAF solutions we start from a global ADAF model with very small \dot{m} . At the outer edge the two ‘standard’ boundary conditions

$$\Omega(R_{out}) = \omega \Omega_K(R_{out}) \quad (23)$$

$$c_s(R_{out}) = \sigma \Omega_K(R_{out}) R_{out} \quad (24)$$

are prescribed, where $0 \leq \sigma \leq 1$ and $0 \leq \omega \leq 1$ are two arbitrary dimensionless constants. In the following, only the case $\omega = 1$ is considered for the sake of simplicity. Once these global ADAF solutions have been computed, \dot{m} is gradually increased up to $\sim 10^{-3}$, each time using the previous model as the input to the next run. For $R_{out} = 10^6 R_g$ this does still not influence the solutions significantly, provided that σ remains close to 1. Starting from these solutions, models with smaller σ are calculated. We find, however, that, owing to the increasing importance of bremsstrahlung cooling, no solution exists below a certain value of σ , which depends on \dot{m} and R_{out} . As soon as

this happens, we move the outer boundary condition for c_s (eq. [24]) to a smaller radius $R_{tr} < R_{out}$,

$$c_s(R_{tr}) = \sigma \Omega_K(R_{tr}) R_{tr} \quad (25)$$

using at the same time a value of σ just above ‘critical’ ($\sigma \sim 0.3$ typically). One of the two outer boundary conditions (eq. [24]) is therefore transformed into an ‘internal’ condition (a constraint which is placed somewhere within the computational domain), which our solver can handle very easily. For any value of R_{tr} we find a global solution which turns out to be an ADAF for $R \lesssim R_{tr}$ and a SLE disk for $R \gtrsim R_{tr}$. We thus obtain a family of SLE–ADAF solutions parametrized by the value of the transition radius R_{tr} .

Our numerical solutions are shown in figure 4, where the disk height is plotted vs. radius for different values of R_{tr} . Bimodal SLE–ADAF solutions have been found previously by Igumenshchev, Abramowicz & Novikov (1997), but, owing to a different choice of the boundary conditions, numerical problems prevented them from computing the entire family of models. The reason is that all solutions are characterized by almost the same value of $H = c_s/\Omega_K$ at the outer edge and, at least those with large enough R_{tr} , also at the inner edge, as can be seen from figure 4. This means that specifying c_s (or H or any other variable) at the outer or the inner edge, instead of the internal condition used here, is formally correct but numerically unstable. Since the problem becomes nearly singular (many solutions with almost the same boundary condition), an impossibly accurate fine tuning would be required for many of the solutions we have found. By setting the condition at the transition radius this problem is solved.

A close-up of the transition region is shown in figures 5, 6, 7 and 8. Details in the behavior of the flow variables in the transition region are of importance inasmuch they can help in shedding light on the physical processes responsible for the transition itself. One of the peculiar features of the transition region is the small peak in the angular velocity which is seen in figure 6. For sufficiently small R_{tr}/R_{max} , as in the model considered here, super–Keplerian rotation may set in. A similar behavior has been found by Honma (1996) in modeling a SSD–ADAF transition with convective flux, and by Igumenshchev, Abramowicz & Novikov (1997). Presumably the super–Keplerian rotation may be attributed to the pressure drop experienced by the gas as it enters the ADAF (Abramowicz, Igumenshchev & Lasota 1997).

5. BIMODAL SLE–SSD FLOWS

In this section we present numerical solutions for bimodal SLE–SSD models. These are disks which are of SLE type for large radii and of Shakura–Sunyaev type for smaller radii. The choice of the parameters is the same as for the solutions discussed in the previous section, $\alpha = 0.1$, $\gamma = 1.5$, $\dot{m} = 10^{-3}$ and $m_* = 10$, although we also tried other values. As in the SLE–ADAF case the transition radius is arbitrary, as long as it is $R_{tr} < R_{max}$. Now, however, we do not construct the full transsonic solutions, and take the inner radius sufficiently far away from the black hole that relativistic corrections are not essential for the flow behavior.

The numerical approach is similar to that outlined in section 4, but now we use the angular momentum equation (11) in its integrated form,

$$\nu R^2 \frac{d\Omega}{dR} = v_R (\Omega R^2 - \ell_0). \quad (26)$$

This reduces the number of first order differential equations from four to three. Since $R_{in} \gg R_g$, the specific angular momentum at the inner edge can be assumed to vanish, $\ell_0 = 0$. We verified that any sufficiently small value is allowed, and found that the results are not very dependent on it.

The SSD part of our bimodal SLE–SSD solutions is optically thick and may be radiation pressure supported. Since the dynamical equations (10, 11, 12) contains the total pressure, rather than the gas pressure, it is not straightforward to compute the gas temperature T from a given value of p (or c_s). In order to get T , equations (2, 3, 4, 5, 14) were solved in a separate iteration loop at each radius for a given value of the total pressure.

5.1. The Boundary Conditions

In contrast to what was discussed in section 4.1, the number of boundary conditions now is three and, since the solution is not transonic, none of them needs to be specified at a critical point this time. At the inner edge we want the flow to be a SSD, so we ask that the radial velocity there attains the value predicted by the standard disk model

$$v_R(R_{in}) = -\frac{\alpha c_s^2(R_{in})}{\Omega_K(R_{in}) R_{in}}. \quad (27)$$

As in the SLE–ADAF case, one boundary condition is given at the outer edge, where the flow is in the SLE phase, and, again, we take

$$\Omega(R_{out}) = \Omega_K(R_{out}). \quad (28)$$

The remaining condition, the one on c_s , needs to be specified at the radius where we choose the transition to occur.

5.2. The Solutions

The way we actually obtained the bimodal SLE–SSD solution is similar to that described in section 4. We started out with a global SLE solution and then worked towards the bimodal solution by slowly modifying the inner boundary condition on the sound speed. By doing so we ran into the same problems as in the SLE–ADAF case, which could only be solved by moving the condition on c_s to a point inside the computational domain, transforming it into an internal condition. The radius at which this condition is specified is again the transition radius. In the present case, however, the numerical integration is much more troublesome because the equations become extremely stiff in the very thin transition region and in the SSD. This is not surprising since the cooling length in the SSD is extremely small, and in the transition region it is even smaller. To circumvent this problem we slightly modified the energy equation to guarantee an artificial lower limit to the cooling length. We believe that this does not invalidate our results, as long as the cooling length remains the smallest length scale of the problem. A particular solution is

shown in figure 9. Contrary to the SLE–ADAF case, now it is very difficult to obtain solutions with a different value of R_{tr} , although possible. For this reason, and also because of the little practical significance of these solutions, we just present here one model.

6. DISCUSSION AND CONCLUSIONS

The goal of this investigation has been to shed some light on the physics of disk transitions. Using a simple argument based on energetics, we have shown that global, stationary bimodal solutions are possible if the outer disk satisfies a simple condition. Our main result is that only an SLE disk can match an inner ADAF (or SSD), while a bimodal accretion configuration formed by an outer SSD and an inner ADAF is not permitted, at least within the standard slim disk physics.

The two allowed bimodal structures, an outer SLE disk glued to an inner ADAF or SSD, have been computed numerically. We found that, in both cases, the transition radius turns out to be arbitrary, so a whole family of solutions exists. This may sound odd, since there is no physical reason to ask the sound speed to take a precise value at an intermediate radius, as we did in finding our numerical solutions. In principle the condition should be placed at the outer edge. In doing so, however, one should be extremely accurate in fixing $c_s(R_{out})$ to find the transition at the desired radius since most bimodal solutions correspond to very nearly identical values of c_s (or any other variable) at the outer or inner edge. It remains nevertheless true that the structure of bimodal disks is determined once a complete set of conditions is prescribed at the edges and

at the sonic radius, without the need of any extra piece of physics.

The existence of the SLE–ADAF and SLE–SSD bimodal solutions agrees with the energy argument of section 3, and strengthens its plausibility. The same argument indicates that a SSD–ADAF model is not allowed. There is a caveat here, however. The essence of the energy argument lies in recognizing that the non–locality of the advective cooling term in the energy equation can be removed by performing a transformation to the fluid frame, and doing the thermal analysis in the frame comoving with the fluid. If, on the other hand, thermal conduction is introduced, the energy equation becomes a second order diffusion type equation and there is no way of removing the non–locality by changing the observer’s frame. In this case our argument definitely does not apply. Honma (1996) has shown that SSD–ADAF structures are possible when the thermal heat flux from the hot ADAF into the SSD is accounted for. In such accretion flows the location of the transition follows self–consistently from the model, contrary to what we have found in this paper. This is because the heat flux will evaporate per unit time an amount of matter from the SSD which needs to be in balance with the actual accretion rate. The transition radius will therefore automatically adjust itself until this balance is reached. In concluding, we would like to state clearly that, because of the thermal instability of the SLE disk, the models presented here most probably do not exist in nature.

We wish to thank I. Igumenshchev, M.A. Abramowicz and R. Narayan for useful comments and suggestions.

REFERENCES

- Abramowicz, M.A., Czerny, B., Lasota, J.–P., & Szuszkiewicz, E. 1988, *ApJ*, 332, 646
 Abramowicz, M.A., Chen, X.–M., Kato, S., Lasota, J.–P., & Regev, O. 1995, *ApJ*, 438, L37
 Abramowicz, M.A., & Lasota, J.–P. 1995, Comments on a Workshop on Slim Accretion Disks and Boundary Layers, astro–1995–05/ITP 95–10
 Abramowicz, M.A., Chen, X.–M., Granath, M., & Lasota, J.–P. 1996, *ApJ*, 471, 762
 Abramowicz, M.A., Igumenshchev, I.V., & Lasota, J.–P. 1997, *MNRAS*, in press
 Chen, X.–M., Abramowicz, M.A., Lasota, J.–P., Narayan, R., & Yi, I. 1995, *ApJ*, 443, L61
 Chen, X.–M., Abramowicz, M.A., & Lasota, J.–P. 1997, *ApJ*, 476, 61
 Esin, A.A., McClintock, J.E., & Narayan, R. 1997, *ApJ*, 489, 865
 Frank, J., King, A., & Raine, D., 1992, *Accretion Power in Astrophysics* (Cambridge: Cambridge Univ. Press)
 Hameury, J.–M., Lasota, J.–P., McClintock, J.E., & Narayan, R. 1997, *ApJ*, 489, 234
 Honma, F. 1996, *PASJ*, 48, 77
 Honma, F., Matsumoto, R., & Kato, S. 1993, *ApJS*, 210, 365
 Ichimaru, S. 1977, *ApJ*, 214, 840
 Igumenshchev, I.V., Abramowicz, M.A., & Novikov, I. 1997, *MNRAS*, in press
 Meyer, F., & Meyer–Hofmeister, E. 1981, *A&A*, 104, L10
 Meyer, F., & Meyer–Hofmeister, E. 1994, *A&A*, 288, 175
 Mineshige, S., & Wheeler, J.C. 1989, *ApJ*, 343, 241
 Narayan, R., & Yi, I. 1994, *ApJ*, 428, L13
 Narayan, R., & Yi, I. 1995, *ApJ*, 452, 710
 Narayan, R., Yi, I., & Mahadevan, R. 1995, *Nature*, 374, 623
 Narayan, R., McClintock, J.E., & Yi, I. 1996, *ApJ*, 457, 821
 Narayan, R., Barret, D., & McClintock, J. 1997, *ApJ*, 482, 448
 Narayan, R., Kato, S., & Honma, F. 1997, *ApJ*, 476, 49
 Nobili, L., & Turolla, R. 1988, *ApJ*, 333, 248
 Paczyński, B., & Wiita, P.J. 1980, *A&A*, 88, 23
 Piran, T. 1978, *ApJ*, 221, 652
 Pringle, J.E., Rees, M.J., & Pacholczyk, A.G. 1973, *A&A*, 29, 179
 Shakura, N.I., & Sunyaev, R.A. 1973, *A&A*, 24, 337
 Shapiro, S.L., Lightman, A.P., & Eardley, D.M. 1976, *ApJ*, 204, 187
 Szuszkiewicz, E., & Miller, J.C. 1997, *MNRAS*, 287, 165
 Szuszkiewicz, E., & Miller, J.C. 1997, *MNRAS*, submitted
 Thorne, K.S., & Price, R.H. 1975, *ApJ*, 195, L101

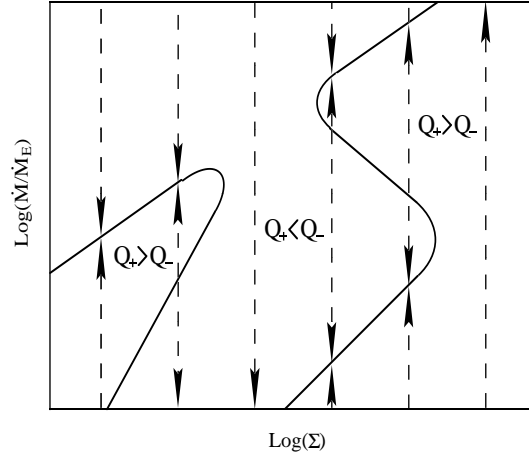


FIG. 1.— Unified picture of accretion flows onto black holes. Solid lines mark the different branches of solutions. A branch is stable when arrows point towards the solid line.

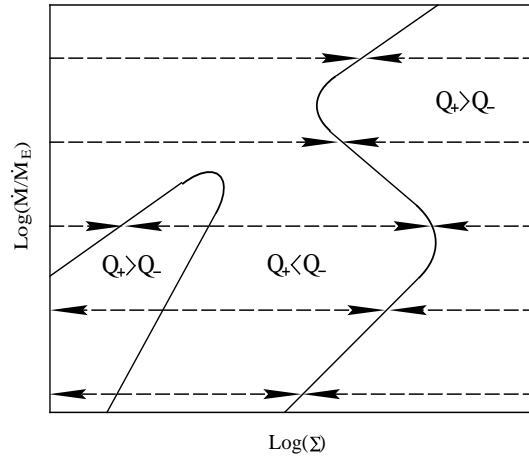


FIG. 2.— Same as in figure 1 for the transition analysis. Stationary, global bimodal models are possible for those solutions which lie on branches with outward pointing arrows. The only option is the SLE branch. The radiation pressure dominated SSD branch is unstable, but cannot change into a hot ADAF in a stationary model.

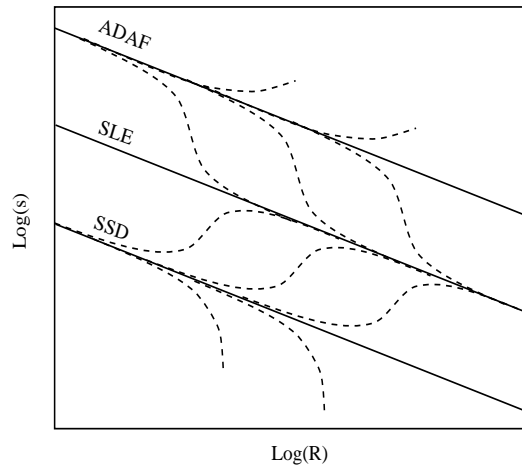


FIG. 3.— A schematic plot of the integral curves (dashed lines) of equation (21). The solid lines are the ADAF, SLE and SSD branches. Each curve is found by starting at some radius with a given specific entropy and integrating inwards. It is clearly seen that integral curves tend to move away from the SLE branch but converge to either the ADAF or the SSD branch.

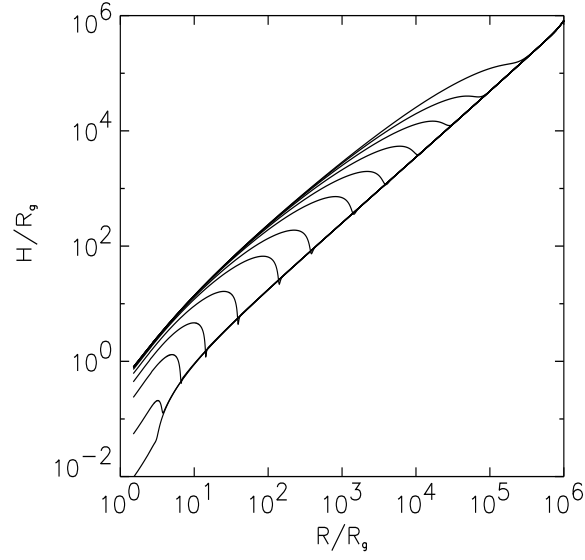


FIG. 4.— The disk geometry for the family of SLE-ADAF models with $\dot{m} = 10^{-3}$, $m_* = 10$, $\alpha = 0.1$ and $\gamma = 1.5$. Each model is characterized by a different location of the transition radius.

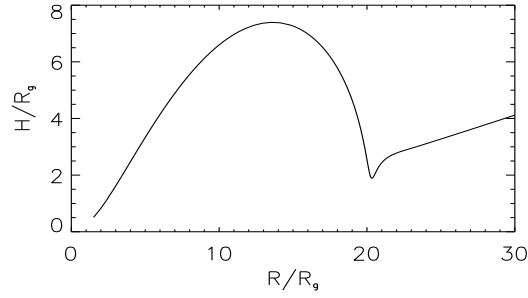


FIG. 5.— Close-up of the transition region for one of the SLE-ADAF transition solutions of figure 4. The star marks the position of the transition radius.

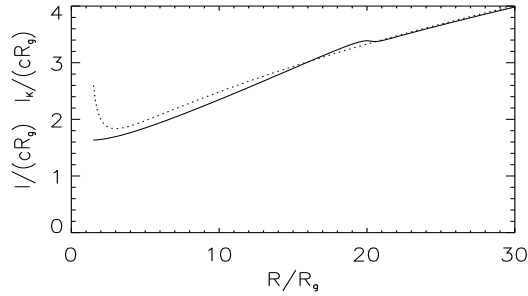


FIG. 6.— Same as in figure 5 for the specific angular momentum (solid line) and for the Keplerian angular momentum (dotted line). Super-Keplerian motion is clearly visible.

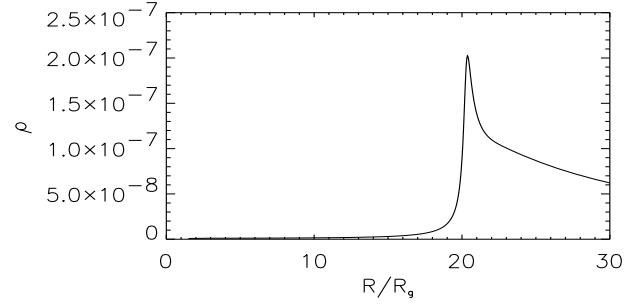


FIG. 7.— Same as in figure 5 for the density (in cgs units).

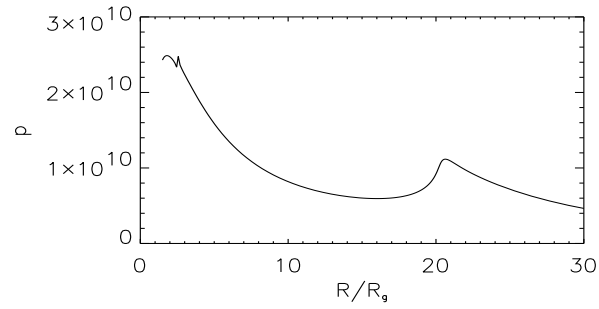


FIG. 8.— Same as in figure 5 for the pressure (in cgs units). The pressure drop as the SLE material enters the ADAF is clearly seen. The small wiggle at the critical point is a numerical artifact and is of no significance.

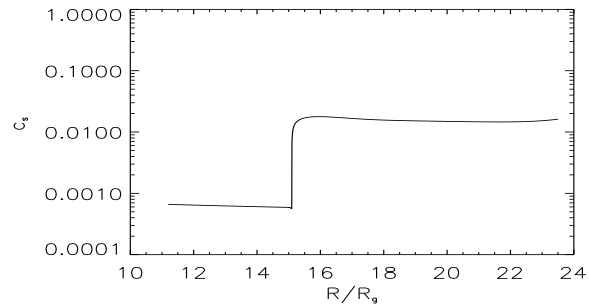


FIG. 9.— The isothermal sound speed (in units of c) for a bimodal SLE–SSD configuration. The star marks the position of the internal boundary condition R_{tr} . The solution is in the SLE phase for $R > R_{tr}$ and in the SSD phase for $R < R_{tr}$.